



This is a repository copy of *Effect of processing route on ballistic performance of Ti-6Al-4V armour plate*.

White Rose Research Online URL for this paper:

<https://eprints.whiterose.ac.uk/205749/>

Version: Published Version

Article:

Fernández Silva, B. orcid.org/0000-0003-2288-9675, Levano Blanch, O. orcid.org/0000-0002-7690-6891, Sagoo, K. et al. (1 more author) (2023) Effect of processing route on ballistic performance of Ti-6Al-4V armour plate. *Materials Science and Technology*, 39 (17). pp. 2910-2920. ISSN 0267-0836

<https://doi.org/10.1080/02670836.2023.2229175>

Reuse

This article is distributed under the terms of the Creative Commons Attribution (CC BY) licence. This licence allows you to distribute, remix, tweak, and build upon the work, even commercially, as long as you credit the authors for the original work. More information and the full terms of the licence here:

<https://creativecommons.org/licenses/>

Takedown

If you consider content in White Rose Research Online to be in breach of UK law, please notify us by emailing eprints@whiterose.ac.uk including the URL of the record and the reason for the withdrawal request.



eprints@whiterose.ac.uk
<https://eprints.whiterose.ac.uk/>

Effect of processing route on ballistic performance of Ti-6Al-4V armour plate

Beatriz Fernández Silva, Oliver Levano Blanch, Kam Sagoo & Martin Jackson

To cite this article: Beatriz Fernández Silva, Oliver Levano Blanch, Kam Sagoo & Martin Jackson (2023) Effect of processing route on ballistic performance of Ti-6Al-4V armour plate, Materials Science and Technology, 39:17, 2910-2920, DOI: [10.1080/02670836.2023.2229175](https://doi.org/10.1080/02670836.2023.2229175)

To link to this article: <https://doi.org/10.1080/02670836.2023.2229175>



© 2023 The Author(s). Published by Informa UK Limited, trading as Taylor & Francis Group.



Published online: 30 Jun 2023.



Submit your article to this journal [↗](#)



Article views: 720



View related articles [↗](#)



View Crossmark data [↗](#)



Citing articles: 1 View citing articles [↗](#)

Effect of processing route on ballistic performance of Ti-6Al-4V armour plate

Beatriz Fernández Silva ^a, Oliver Levano Blanch ^a, Kam Sagoo^b and Martin Jackson ^a

^aDepartment of Materials Science and Engineering, University of Sheffield, Sheffield, UK; ^bRheinmetall BAE Systems Land (RBSL), Hadley Castle Works, Telford, UK

ABSTRACT

Titanium alloys are a key part of an armour designer's toolset due to their high ballistic mass efficiency. However, titanium's high cost has restricted its use in military land-based vehicles. In this study, the effect of different processing routes on the microstructure, texture, ballistic performance V_{50} and deformation modes of Ti-6Al-4V armour plate is investigated. Plates were fabricated via conventional hot rolling and the powder metallurgy techniques of HIP and FAST. The plate failure modes varied significantly with the microstructure while the formation of adiabatic shear bands seems to be influenced by crystallographic texture. The rolled plate exhibited the best performance due to a strong transverse-type texture perpendicular to the projectile direction.

ARTICLE HISTORY

Received 28 December 2022
Revised 12 May 2023
Accepted 20 June 2023

KEYWORDS

Ti-6Al-4; ballistic performance; microstructure; texture; processing

Introduction

The use of titanium alloys within the defence sector is advantageous due to its weight-to-strength ratio, particularly for structural applications. Owing to the high ballistic mass efficiency of armour grade Ti-6Al-4V alloy, compared with Rolled Homogeneous Armour (RHA) steel, 30–40% weight reductions can be achieved, and no additional appliqué armour is required [1]. With the implementation of the MIL-A-46077 military specification for armour components of Ti-6Al-4V and its use in combat vehicles [2], more research has been done on understanding the impact performance of titanium alloys manufactured by conventional methods [3–5]. However, the prohibitive cost of titanium alloys, up to 20 times the cost of RHA steel, together with the lack of knowledge about its ballistic properties in the early stages, have prevented their use on armour applications.

The increase of the oxygen content to a maximum of 0.30% established by the MIL-DTL-46077G [6] specification for military applications allowed the use of lower-cost single melting technologies such as Electron Beam or Plasma Melting processes [5]. Albeit, energy and labour-intensive thermomechanical processing by hot rolling is still required. Powder metallurgy (PM) routes were also considered with the added advantage of the possibility to obtain a near-net shape component. The blended elemental (BE) PM approach has seen high volume production in the missile industry, such as in sparrow missile wings [7]. ADMA Products, Inc. produced titanium plates using TiH₂ powders via Cold Isostatic Pressing and rolling [8]. International Titanium Powder (ITP) produced CP-Ti and Ti-6Al-4

V plates via Vacuum Hot Pressing (VHP) using Armstrong powders [9]. In both cases, the ballistic performance was similar to conventional wrought Ti-6Al-4V properties for specific thickness of plate. However, the cost of production and/or post-processing required for the powder feedstock of this BEPM approach is still the main limiting factor for their consideration as low-cost PM processes for the manufacture of titanium products.

Alternatively, Hot Isostatic Pressing (HIP) and Field Assisted Sintering Technology (FAST) are direct solid-state consolidation techniques that enable near-net shapes to be produced in one single step, using vacuum or protective atmospheres, with the proven capability to use lower-cost titanium powder and particulate feedstock in the FAST process [10–13]. HIP is the most common method used for consolidating titanium alloy powders, which are hermetically sealed in a mild or stainless steel can [14]. The pressure is applied isostatically to canned powder using argon gas at furnace temperatures around 900°C heated by convection.

The work by Nesterenko et al [15,16] on the investigation of HIP using Ti-6Al-4V plasma rotating electrode process powder showed enhanced ballistic performance when compared to conventional rolled plate material. The FAST process consolidates powder by heat, via the joule effect of an electric current in graphite dies, and mechanical pressure. Compared to HIP, it allows shorter processing times, and the reutilisation of the graphite dies and tooling [17]. However, the ballistic performance of titanium billets produced from powder via FAST has not been previously investigated.

CONTACT Beatriz Fernández Silva  b.silva@sheffield.ac.uk  Department of Materials Science and Engineering, University of Sheffield, Sir Robert Hadfield Building, Mappin St, Sheffield S1 3JD, UK

In titanium alloys, microstructure and texture are strongly dependant on thermomechanical processing parameters [18–20]. For armour applications, thermomechanical processing significantly influences ballistic performance [21]. Beta processed material exhibits low-energy absorption with a dominant failure mode of adiabatic shear plugging, while $\alpha+\beta$ processed material fails by higher energy absorbing failure modes of enhanced bulging, planar delamination cracks and adiabatic shearing [3]. The higher energy absorption, delamination crack failure modes of the $\alpha+\beta$ processed material established by Burkins et al [4] was later linked to a strong transverse texture [22]. Similarly, recent research in other hexagonal close-packed (HCP) alloys have shown that a transverse texture is beneficial by enhancing energy absorption and restricting strain hardening [23]. The type of failure mechanisms has also been linked to the microstructure and the propagation of the adiabatic shear bands that lead to ductile or brittle failure for bimodal or lamellar microstructures, respectively [24–26]. Compared to HIPed Ti-6Al-4V, the differences in ballistic performance and different shear bands patterns are believed to be related to the difference in texture [27]. However, previous investigations on the effects of texture on ballistic performance by Kad et al [28] and Schoenfeld et al [22] did not explicitly measure the texture of the ballistically tested material and instead assumed generalised processing and recrystallisation textures from the literature.

In this investigation, different processing routes of Ti-6Al-4V plates and their microstructure, texture and ballistic performance were fully characterised. The main objective is to compare the performance and failure modes of the baseline material processed by conventional rolling to alternative powder metallurgy routes such as conventional HIP and field-assisted sintering technology (FAST).

Materials and methods

Plate processing routes

The materials used in this investigation are Ti-6Al-4V plates with thicknesses of 14.2, 13.8 and 12.7 mm processed via conventional rolling, FAST and HIP, respectively. The rolled plate is ASTM 256 Ti-6Al-4V Grade 5 in the mill-annealed condition. Two FAST plates of 250 mm diameter were produced using surplus Ti-6Al-4V powder using The University of Sheffield's FCT HP

D250 machine, where a large amount of prior research has been carried out into the consolidation of titanium particulates via FAST [13,17,29,30], using a sintering cycle of 30 min dwell time at 1100°C or 950°C with a uniaxial pressure of 35 MPa, with no further heat treatment. The HIPed plate was manufactured by BAE Systems to a proprietary BAE Systems HIP cycle. After sintering the HIPed plate was then stress relieved to a 'mill anneal' temperature, so it is comparative with commercial mill annealed wrought titanium products. Table 1 shows the composition of the Ti-6Al-4V products or feedstock (in the case of FAST and HIP processing) used in this investigation.

Ballistic impact experiments

The plates were used as targets for the V_{50} ballistic impact experiments conducted by RBSL to obtain the V_{50} ballistic limit of the plates according to the MIL-STD-662F specification for evaluating armour materials using a threat of 30-cal APM2 Armour-piercing projectile. A schematic of the setup is shown in Figure 1. Between 9 and 12 shots were fired into each plate with velocities starting at 30 m/s above the minimum required V_{50} given in the MIL-DTL-46077G specification [31]. The V_{50} indicates the velocity of the bullets where 50% of the bullets penetrates the target. In this study, a failure is considered when damage is caused in the witness card placed behind the target, see Figure 1 with the red line. A pass occurs when the projectile is contained by the target or when no light can be seen through the witness card, see Figure 1 with the blue line.

The attack and rear faces of the perforated plates were photographed. Pass and fail shots were selected from each plate and sectioned parallel and across the penetration direction for further examination (Section 2.3).

Texture and microstructure analysis

The analysis of microstructure and texture in the bulk material was performed in the transverse plane of each plate. Note that in all cases, the transverse plane is parallel to the projectile direction. The specimen surface was ground, polished and etched using Kroll's reagent to reveal the microstructure for optical microscopy. Micrographs were obtained using Olympus Bx51 with the software Clemex Vision PE. The texture analysis

Table 1. Chemical composition and powder size distribution of the Grade 5 Ti-6Al-4V materials used for the manufacture of each product and composition requirement for MIL-DTL-46077G titanium armour specification [6,36].

	Powder size (μm)	O	C	N	H	Comments
Class 2 (MIL-DTL-46077G)	n/a	0.2	0.08	0.05	0.0150	Common Armor: 6% Min Elongation
Ti-6Al-4V Grade 5	n/a	0.20	0.08	0.05	Max 0.015	Rolled plate
PREP powder	60–123	0.18	0.04	0.008	0.0032	FAST-1100
GA powder	105–405	0.12	0.004	0.008	0.0019	FAST-950
PA powder	45–180	0.12	0.01	0.01	0.001	HIP

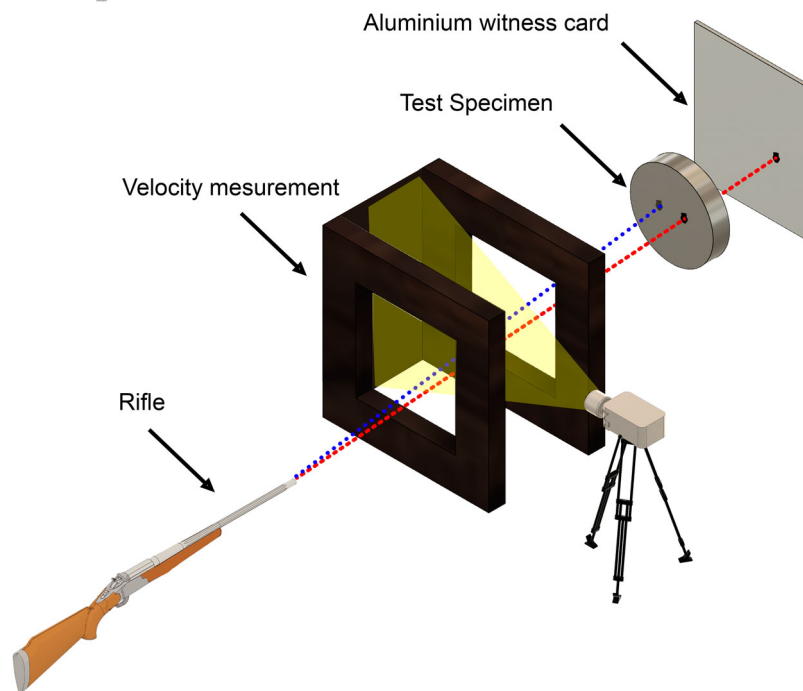


Figure 1. Schematic setup of the ballistic experiments were the dotted lines show the trajectory of two different projectiles. The red dotted line represents a failure of the material, and the blue dotted line represents a pass.

was performed by electron backscattered diffraction in a scanning electron microscope JEOL7900F equipped with a Symmetry detector and AZtecHKL. Post-processing of the texture data was performed using the open access MTEX [32]. Post-ballistic investigation was performed by optical microscopy in the cross section of selected targets perpendicular to the projectile direction after etching. The hardness was measured with a Vickers Armstrong Pyramid Testing Machine 3290 at HV30.

Results and discussion

Microstructure of the Ti-6Al-4V plates

The microstructure from the bulk material of the Ti-6Al-4V plates is shown in Figure 2. The rolled plate shows a bimodal microstructure of primary alpha grains (α_p) and secondary alpha colonies (α_s) with 50% volume fraction of α_p grains of 20 μm diameter, Figure 2(a). The microstructure from HIP (Figure 2(b)) and FAST-950°C (Figure 2(d)) material shows a quasi-equiaxed microstructure consisting of alpha nodules and thick alpha laths of 3–10 μm width being coarser for HIP material. The FAST-1100°C plate shows the typical β -processed fully lamellar microstructure with grain sizes between 200 and 500 μm diameter surrounded by grain boundary alpha of 10–20 μm thick and alpha lath widths of the lamellar colony structure between 3 and 6 μm (Figure 2(c)). The highest hardness values were found at the fully lamellar microstructure of FAST-1100°C with 360HV30, see Figure 2.

Note that the axial axis AD, and the transversal axes TD₁ and TD₂ are used to relate the reference axis of interest during processing and during ballistic experiments (see axis in Figure 2). For FAST material, AD is parallel to the direction of the uniaxial pressure during sintering while TD₁ and TD₂ are two random orthogonal radial directions of the 250 mm diameter plates. For rolled plate, TD₁ is aligned with the rolling direction. Since the HIP plate was processed under isostatic pressing conditions, no reference axes of interest are allocated. Note that in all cases, AD is parallel to the projectile direction during the ballistic experiments.

V₅₀ ballistic limit results

Table 2 summarises the results from the ballistic trials listing the manufacturing process, heat treatments, and thickness of each target. All plates passed the ballistic impact requirements of MIL-A-46077G except for target FAST-1100°C. Most data points from the tests performed in this work are equal if not better than the base line of the specification MIL-A-46077G, Figure 3. Based on normalised thickness, the rolled plate material was 3.5% better than the minimum required V₅₀, followed by a 1.5% and 1.6% increase for the FAST-950°C and HIP plates respectively, while the FAST-1100°C plate was 0.33% lower than the V₅₀ limit line.

Failure modes from V₅₀ ballistic limit testing

Photographs taken from the attack and rear faces from selected impacts are shown in Figure 4. A pass and

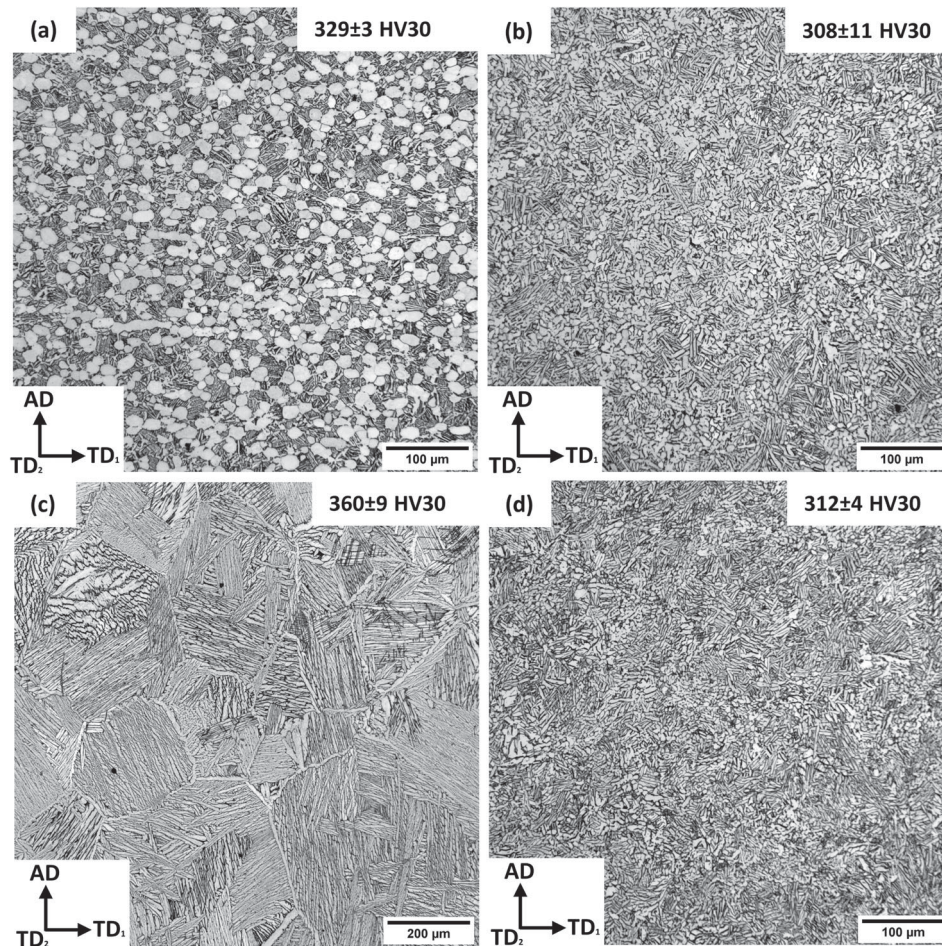


Figure 2. Light optical micrographs from the bulk material of Ti-6Al-4V (a) Rolled plate, (b) HIP plate, (c) FAST-1100°C plate and (d) FAST-950°C plate with their respective HV30 hardness values.

Table 2. Summary of the V_{50} ballistic limit results.

Manufacturing process	Heat treatment	Thickness (mm)	Areal Density (kg/m ²)	V_{50} (m/s)	Std Dev (m/s)	Velocity Spread (m/s)	Required V_{50} (MIL-DTL-46077G) (m/s)
Rolled plate	Mill Anneal	14.2	61.45	704.5	4	10	680.3
HIP ~ 900°C	Mill Anneal	12.7	55.72	641.6	7	16.6	632.1
FAST 1100°C	n/a	13.8	61.17	667.8	6.2	17.6	670.0
FAST 950°C	n/a	13.8	60.57	680.9	6.4	16.8	670.0

a fail were chosen for each plate condition for further investigation. Significant differences in the failure mode are observed between the materials processed in the $\alpha+\beta$ and the β regions which can be directly related to the final microstructure. The bimodal and semi-equiaxed microstructures from $\alpha+\beta$ processing showed a more ductile failure mode with petaling occurring at the front face in both pass and fails, Figure 4(a,b,d). The fully lamellar microstructure resulting from β processing, observed in the FAST-1100°C plate, showed a brittle type of failure by plugging and fragmentation, Figure 4(c-i,c-ii). However, this sample also showed more radial confinement of the bullet, Figure 4(c-iii,c-iv), compared to the other conditions (especially Figure 4(d-iii,d-iv)). This means that less material has fractured and been ejected away from the bullet surroundings, creating a smaller diameter shallow crater on the attack face. The reason why there

is more radial confinement in β -processed materials could be due to the higher fracture toughness behaviour compared to material processed in the $\alpha+\beta$ region. It has been well-documented in the aerospace industry that a large-grained, fully lamellar microstructure provides enhanced crack growth resistance [33].

Adiabatic shear band formation and fracture

As shown in previous ballistic metallography investigations [4,24,25,28], the failure mode is first defined by the microstructure. Adiabatic shear parallel to the direction of impact is commonly observed in all types of microstructures prior to ultimate breakthrough target [22]. The cross sections of each pass from Figure 4 are shown in Figure 5 with highlighted regions to illustrate the deformation by adiabatic shear bands – white ribbon-shaped features – close to the penetration

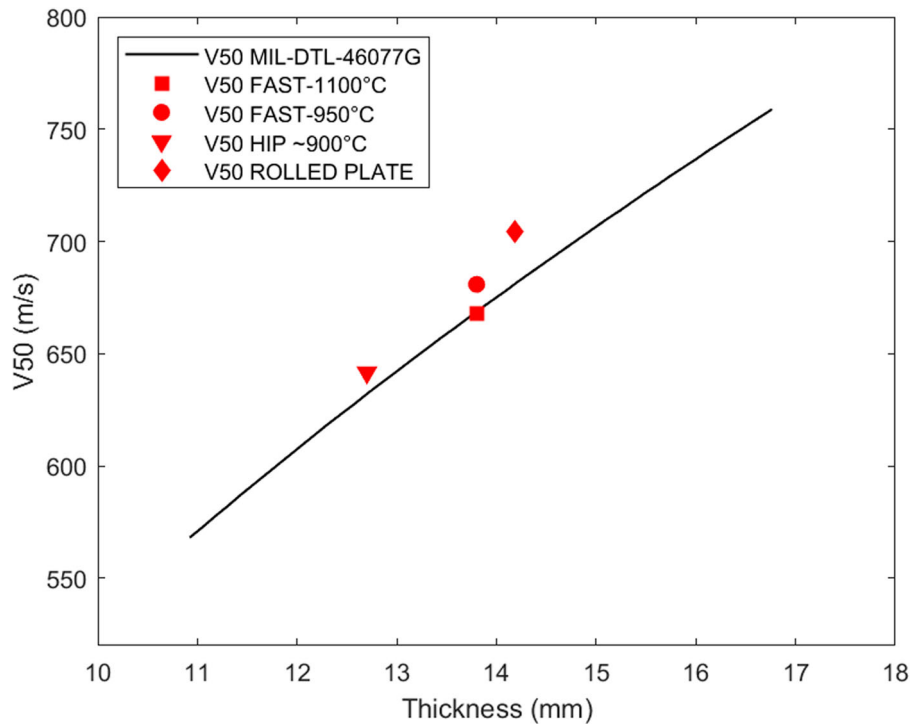


Figure 3. V_{50} against thickness plot comparing the MIL-DTL-46077G minimum required limit line with the experimental results on the four different Ti-6Al-4V plate targets.

hole. The brittle fragmentation previously observed in Figure 4(c–i) for the lamellar microstructure target can also be seen in the cross section (Figure 5(e)) by the spalled fragments that are pulled out from the target. Whereas in bimodal and quasi-equiaxed microstructure a ductile hole formation was observed, particularly for rolled plate and FAST-950°C (Figure 5(a,g)). Adiabatic shear bands (ASB) and ASB-induced cracks are observed in all targets. Such ASBs are considered the major mechanism by which titanium alloys fail and fracture during impact testing [25]. ASBs are generated at high strain rates, and due to the poor thermal conductivity of titanium, leading to adiabatic heating which causes material softening and strain localisation. All targets showed well-defined ASB with varying thickness, propagation directions, ramifications and ASB-induced cracks. The average thickness of the ASBs was about 9–15 μm (rolled plate), 6–18 μm (HIP), 15–20 μm (FAST-1100°C) and 5–13 μm (FAST-950°C) with the thickest ASBs of about 25–30 μm observed in the FAST-1100°C and HIP material, respectively. The length of the ASBs was obtained by measuring the ASB in a straight line from the surface of the hole until the ASB faint in the bulk material. The average length values were about 4 mm (rolled plate), 3.1 mm (HIP), 2.7 mm (FAST-1100°C) and 3.7 mm (FAST-950°C) with the longest ASBs observed in rolled and FAST-950°C plates of 6.3 and 5.6 mm respectively. The rolled plate showed fine and equidistant ASB with a preferred propagation direction following the flow lines of the material inherited from the rolling process, (Figure 5a,b). In the rolled plate, there is a greater

number of ASB which are distributed mainly on the lower half of the cross section in Figure 5(a), showing signs of delamination as highlighted by the white arrow showing a region with an ASB-induced crack. Delamination occurs following the flow path of rolled plate perpendicular to projectile direction through regions of heavily different critical resolved shear stress (CRSS), i.e. soft to hard regions in rolled plate. This has been suggested as an additional failure mechanism allowing for the increased absorption of projectile energy [22] as observed in the rolled plate investigation by Burkins et al [4]. The delamination phenomenon was not observed in any powder-derived Ti-6Al-4V targets, most likely due to the lack of a strong texture anisotropy that generates these regions with significantly different CRSS. As the ASBs are regions of intense plastic instability leading to fracture, the rolled plate distributes this plastic deformation (and thus, energy absorption) over a larger number of thin ASBs compared to the other plate conditions. For example, at the other extreme, the FAST-1100°C processed material, with a large-grained, lamellar structure has a smaller number but thicker ASB, concentrated towards the back end of the plate. Thicker ASB are regions of a higher volume of intense, plastic instability regions – and more prone to fracture. This accounts for the fracture and inter-ASB cracks observed at the back face of the FAST-1000°C plate (Figure 5(e)). The subtle difference between HIP and FAST-950°C material is the slightly larger number of regularly spaced ASB generated in FAST-950°C (Figure 5(g)) compared to HIP (Figure 5(c)), as well as the slightly longer nature of the ASBs for FAST-950°C. Such

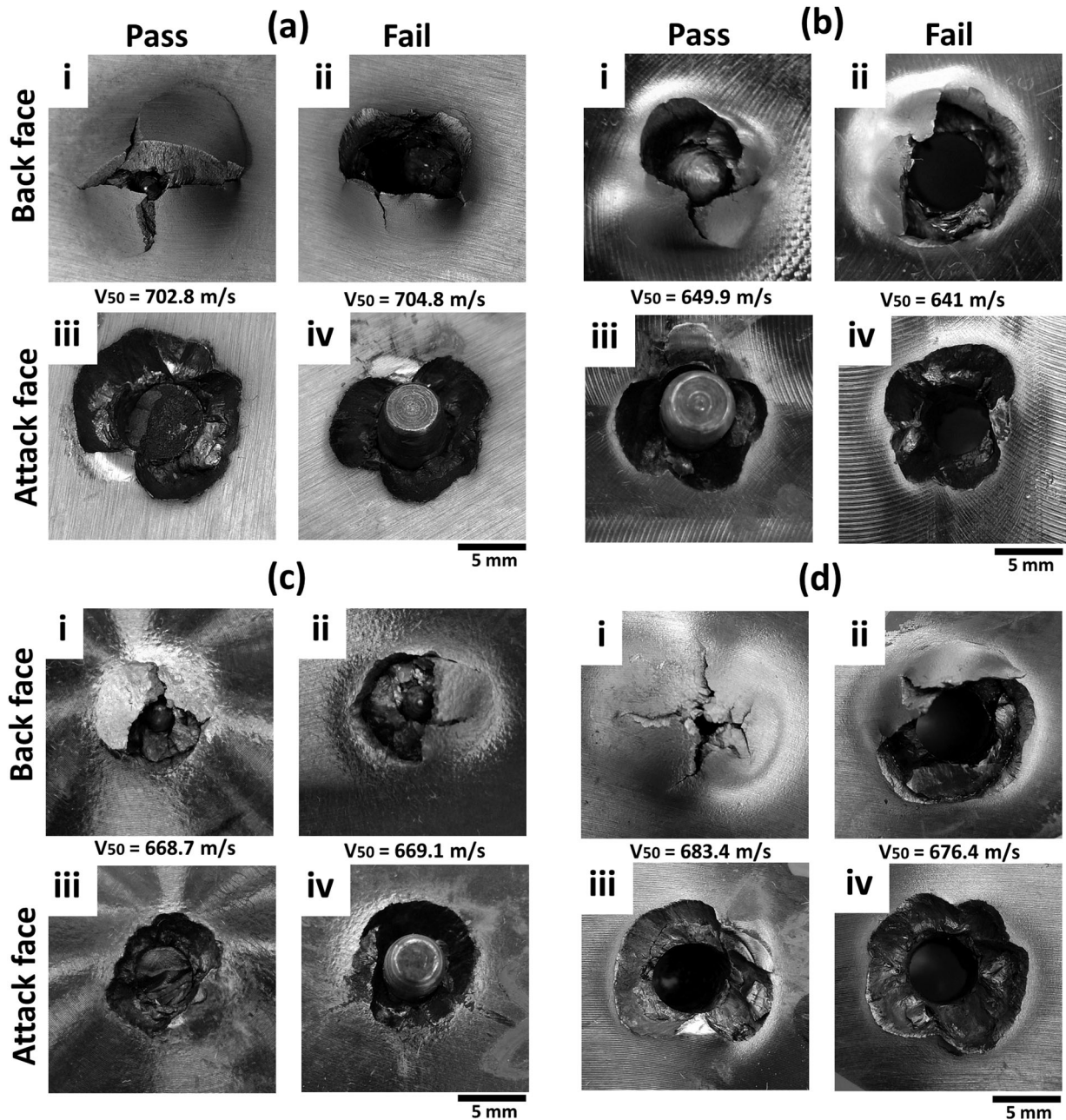


Figure 4. Photographs of the attack (back) and rear (front) face of the impacted targets of Ti-6Al-4V (a) Rolled plate, (b) HIP plate, (c) FAST-1100°C plate and (d) FAST-950°C plate showing pass (i, iii) and fail (ii, iv) ballistic impact from each plate. V_{50} value is indicated for each impact.

ASB in the former are also slightly thinner which again may account for the slightly less fracture in the back end compared to the HIP plate, where the thicker ASB has led to slightly more pronounced cracking/inter-ASB cracking and thus more fragmentation at the back end (Figure 5(c)).

Texture and anisotropy developed in Ti-6Al-4V plates from different processing routes

Orientation maps from the bulk material of the Ti-6Al-4V plates are shown in Figure 6. Inverse pole figure (IPF) orientation maps with respect to the projectile (AD), which is in the vertical axis. The orientation maps show no preferential orientation for the HIP

(Figure 6(b)) and FAST material (Figure 6(c,d)) while a strong anisotropic texture is observed in the rolled plate (Figure 6(a)) displaying band-like features perpendicular to AD which is also highlighted by the respective pole figures (see Figure 7(a)). The pole figure plots of these maps are shown in Figure 7 with respect to the projectile direction (AD in the centre). The rolled plate shows a transverse texture dominated by a strong basal {0002} texture in TD_2 typically observed in hot rolling of titanium alloys [34]. Another lower intensity peak is aligned with TD_1 in the basal {0002} pole figure as a result of cross rolling. Overall, there is no basal component in AD meaning that the c-axis of the HCP crystal, i.e. [0001] direction, is perpendicular to the projectile direction (AD), Figure 7(a). The

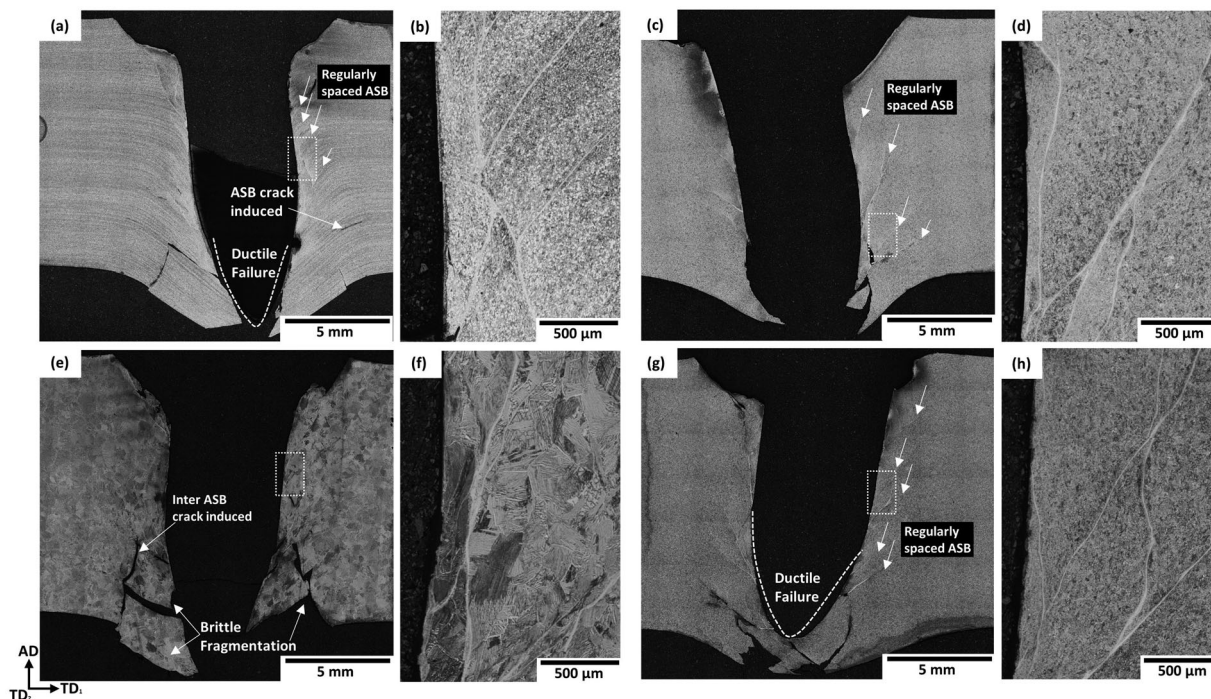


Figure 5. Light optical micrographs mosaics from the etched cross section of pass impacts in Figure 4 and examples of ABS formation and bifurcation near the penetration channel of (a, b) Rolled plate, (c, d) HIP plate, (e, f) FAST-1100°C and (g, h) FAST-950°C plates.

pole figure plots from HIP plate and FAST-1100°C plate show a non-descriptive texture with several intensity peaks with no preferential alignment with any reference axis, Figure 7(b,c). Contrastingly, the FAST-950°C plate shows a weak compression texture, as represented in the basal {0002} pole figure with the c-axis lying perpendicular to the projectile direction (AD) showing some preferential alignments in three radial directions, Figure 7(d).

The influence of texture on ballistic performance

The texture analysis has shown that there are two main types of texture within the Ti-6Al-4V targets investigated in this work: having the c-axis of the HCP crystal either perpendicular or not with respect to the projectile direction. The rolled plate showing the best ballistic performance has the c-axis lying perpendicular to the projectile direction (Figure 7(a)) as a result of

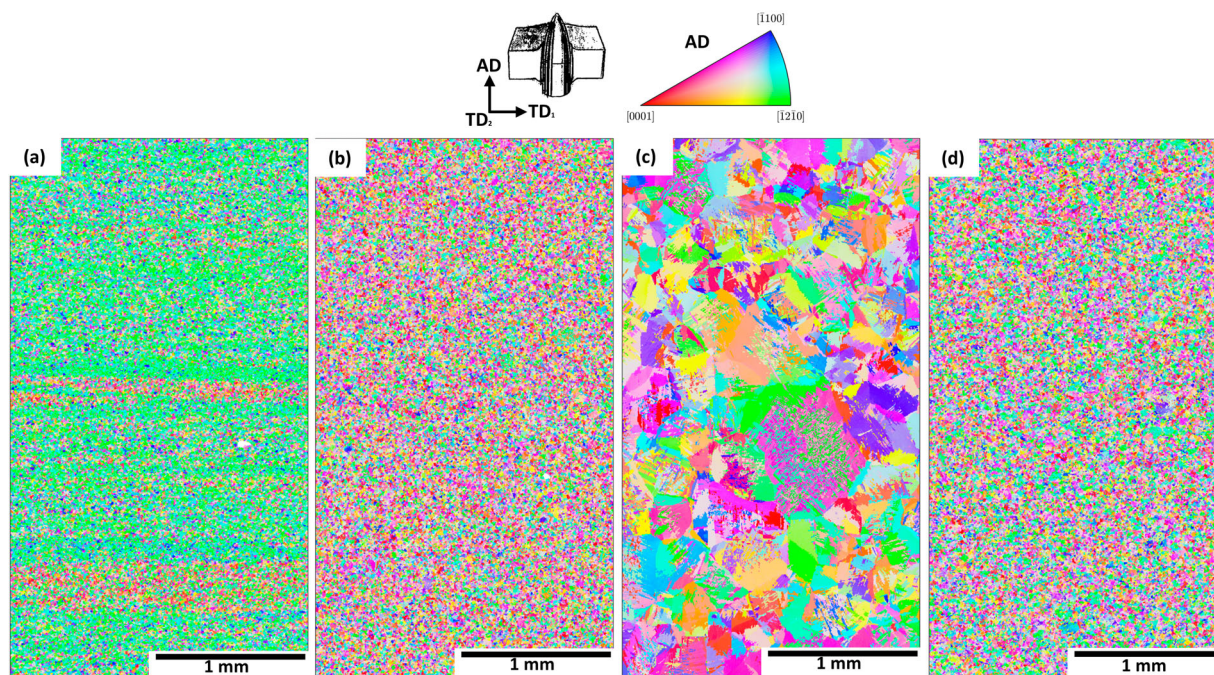


Figure 6. Inverse pole figure (IPF) orientation maps with respect to the axial direction (AD) from the bulk material of Ti-6Al-4V (a) Rolled plate, (b) HIP plate, (c) FAST-1100°C plate and (d) FAST-950°C plate.

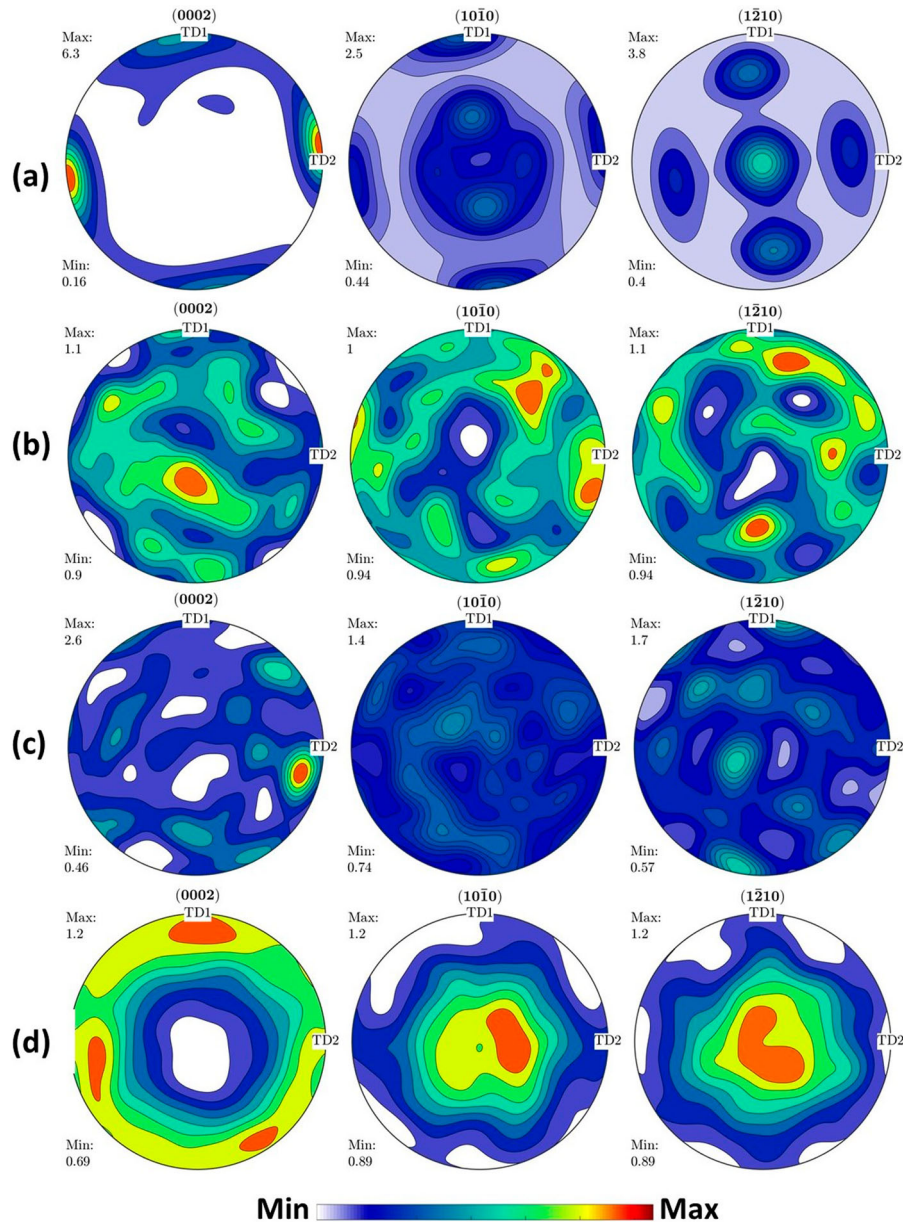


Figure 7. Basal {0002}, Prismatic $\{10\bar{1}0\}$ and $\{1\bar{2}10\}$ pole figure plots from the bulk material of Ti-6Al-4V (a) Rolled plate, (b) HIP plate, (c) FAST-1100°C plate and (d) FAST-950°C plate. AD is in the centre of the pole figures which is parallel to the projectile direction.

the transverse type texture developed from the rolling process. This is also the case for the FAST-950°C plate although in this case this is a result of a weak compression texture inherited from the uniaxial pressure direction in the sintering/consolidation process when processing below T_β , Figure 7(d). This agrees with ballistic work performed in magnesium alloys at which a transverse texture exhibits enhanced ballistic performance when the c-axis is perpendicular to the projectile direction by the increment of slip activity in contrast to the strong basal texture [23]. However, this is not the case for the HIP plate due to the isostatic pressure being applied in all directions during the consolidation process, resulting in a random texture. Despite the differences in the microstructure, the texture in HIP

is similar to the texture observed in the FAST-1100°C plate, Figure 4 (b,c).

For the transverse and compression texture of rolled plate and FAST-950°C plate, respectively, the deformation by impact of the projectile is likely to occur mainly in soft prismatic planes. This is shown schematically in Figure 8(b) at which the c-axis of the HCP crystal is lying perpendicular to the shooting direction. While in HIP and FAST-1100°C plate, the random distribution, although it is commonly desirable to obtain isotropic properties in titanium alloys, might lead to a lower density of crystals preferentially aligned for deformation to occur due to the wider range of orientations covered. This is due to the strong anisotropic behaviour of the HCP crystal of the titanium α -phase with respect to the

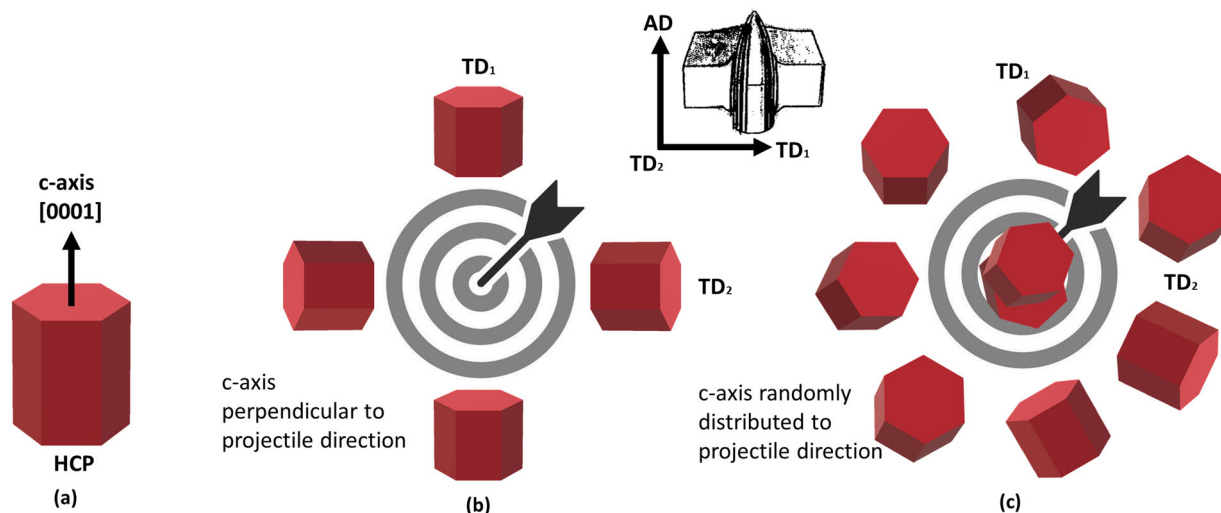


Figure 8. Schematic drawing of the distribution of the (a) HCP crystals with respect to the projectile direction for (b) Rolled plate and FAST-950°C plate, and (c) HIP and FAST-1100°C plate.

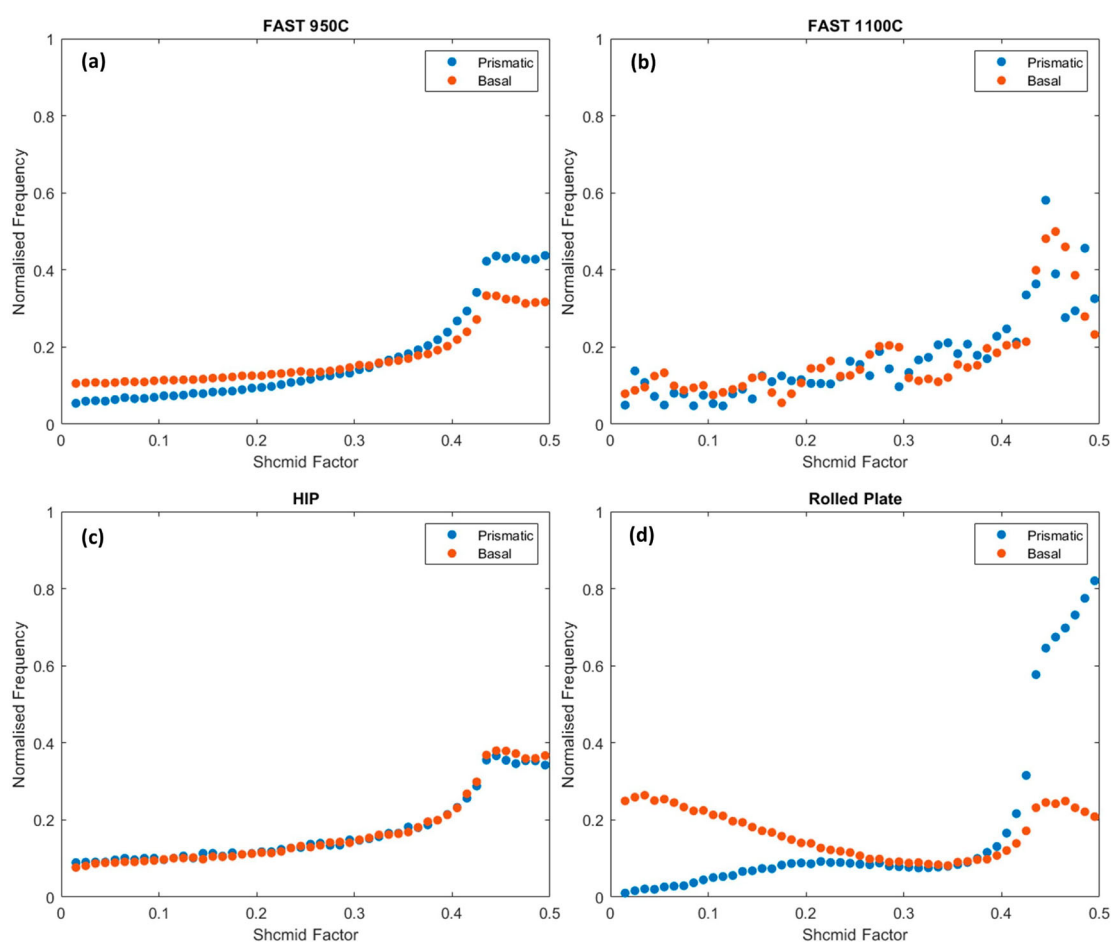


Figure 9. Schmid factor distributions for the basal (a) and prismatic (a) slip for the (a) FAST-950°C (b) FAST-1100°C (c) HIP plate and (d) Rolled plate.

main loading direction (i.e. projectile direction in the current investigation) [35]. In this case, the HCP crystals had the c -axis not only lying perpendicular to the shooting direction but also parallel or to an angle with respect to the shooting direction, as shown schematically in Figure 8(c).

A detailed Schmid Factor (SF) quantification was obtained from the orientation EBSD datasets to predict

the likelihood on deformation behaviour on the different materials for Basal and Prismatic slip systems, Figure 9. The Schmid factor distribution for the rolled plate material suggests that there is a high density of grains preferentially orientated for Prismatic (a) slip, Figure 9(d), in contrast to the other materials which showed similar tendencies for Basal (a) and Prismatic (a) slip at low and high SF values but with lower

frequencies, i.e. less grains orientated favourably for slip to occur. Note, however, that the Schmid factor distribution for HIP (Figure 9(c)) and FAST-950°C (Figure 9(a)) plates follow the same trend but there is a slightly higher preference for Prismatic $\langle a \rangle$ slip activation on the FAST-950°C plate, which could explain the subtle differences in the ballistic performance of the FAST-950°C versus HIP material. Despite the similar observed availability of both Basal $\langle a \rangle$ and Prismatic $\langle a \rangle$ activation on the FAST-1100°C (Figure 9(a)) at relatively high SF values, the effect of a fully lamellar microstructure on the failure mode appears to have a bigger influence than the texture present in the material.

The SF analysis suggests that the easier activation of Prismatic $\langle a \rangle$ slip in rolled plate plays an important role on the enhanced ballistic performance of this material compared with the other targets in the current work. This is due to the rolling texture inherited from the processing of the rolled plate leading to the presence of a large number of grains favourably orientated for Prismatic $\langle a \rangle$ slip to occur, i.e. the c -axis is perpendicular to the shooting direction, as shown in Figure 8(b), and therefore the prismatic planes are subject to a high critical resolved shear stress (CRSS), while basal planes will have very low or none CRSS as shown in Figure 8(d). This, however, was not the case for the other materials (particularly HIP and FAST-1100C) whose HCP crystals had the c -axis in all directions, as shown by the pole figures in Figure 7(b,c) and Figure 8(c). Those textures have shown a smaller number of grains favourably orientated for slip (Basal $\langle a \rangle$ and Prismatic $\langle a \rangle$) compared to the rolled textured target which suggests that these are less prone to plastically deform under loading and therefore less energy absorption diminishing their ballistic performance.

Conclusions

Ti-6Al-4V targets produced from conventional titanium mill products and alternative powder metallurgy routes were successfully tested against ballistic performance. The targets including rolled and HIP plates, and a FAST plate performed successfully according to the MIL-A-46077G specification when processed in the $\alpha + \beta$ region. The target processed by conventional rolling, commonly used as baseline in ballistic testing of titanium alloys, exhibits the best performance followed by the FAST and HIP products. Post-ballistic investigation suggests that while the fulfilment of the V_{50} requirement might be defined by the microstructure resulting from the processing temperature with respect to T_{β} in titanium alloys, the deformation mode leading to ASB propagation, density and thickness and ultimately, leading to failure is texture dominated. This work has shown that the c -axis distribution and orientation of the HCP crystals plays a key role in the

deformation behaviour with respect to the projectile direction.

In the current work, the texture resulting from the processing can generate this optimum texture for ballistic performance in rolled plate and FAST using surplus Ti-6Al-4V powder from their rolling and compression texture regarding the projectile direction respectively. While in the rolled plate this is a result of the rolling texture, in the FAST-950°C plate this is generated by a weak compression texture inherited from the uniaxial pressure direction in the sintering process. This, however, is not the case for the HIP process due to the sintering pressure being applied in all directions, resulting in a random texture, i.e. random distribution of the c -axis. This, together with the adding value of the low-cost nature of the process by (1) the use of surplus commercial titanium alloys powder (2) short sintering cycles compared to HIP and (3) the no need for a post heat treatment place the FAST process as a good candidate to reduce cost and enhance sustainability for the production of titanium components.

Acknowledgements

This research was co-funded by Dstl by ATITUDE – Affordable Titanium for Defence programme DSTLX-1000148418 and EPSRC through grant EP/T024992/1 and for the FAST capability as part of the Henry Royce Institute (grant EP/R00661X/1). The authors acknowledge RBSL and BAE Systems for performing the ballistic experiments and providing the HIP plate respectively. We also acknowledge Neil Middleton (Dstl), Dr Matthew Lunt (Dstl) and Peter Stewart (BAE Systems) for useful discussions.

Disclosure statement

No potential conflict of interest was reported by the author(s).

Funding

This work was supported by Defence Science and Technology Group [grant number DSTLX-1000148418]; Defence Science and Technology Laboratory [grant number DSTLX-1000148418]; Engineering and Physical Sciences Research Council [grant number EP/T024992/1; EP/R00661X/1].

ORCID

Beatriz Fernández Silva  <http://orcid.org/0000-0003-2288-9675>

Oliver Levano Blanch  <http://orcid.org/0000-0002-7690-6891>

Martin Jackson  <http://orcid.org/0000-0002-9553-1239>

References

- [1] Montgomery JS, Wells MGH, Roopchand B, et al. Low-cost titanium armors for combat vehicles. *JOM*. 1997;49:45–47. doi:10.1007/BF02914684
- [2] Montgomery JS, Wells MGH. Titanium armor applications in combat vehicles. *JOM*. 2001;53:29–32. doi:10.1007/s11837-001-0144-2

- [3] Burkins MS, Hansen JS, Paige JJ, et al. The effect of thermo-mechanical processing on the ballistic limit velocity of extra low interstitial titanium alloy Ti-6Al-4V, ARL-MR-486., 2000.
- [4] Burkins MS, Love WW, Wood JR. Effect of annealing temperature on the ballistic limit velocity of Ti-6Al-4V ELI, 1997. doi:10.1080/02670844.2019.1587141.
- [5] Gooch WA. The design and application of titanium alloys to U.S. Army Platforms -2010, TITANIUM 2010 International Titanium Association. 2010.
- [6] MIL-DTL-46077G, Armor plate, Titanium alloy, Weldable, 2006.
- [7] Abkowitz S, Fujishiro S, Eylon D, et al. Titanium alloy shapes from blended elemental powder and tensile & fatigue properties of low chloride composition, in: Titan. Net Shape Technol., 1984: p. 107–120.
- [8] Adams JW, Duz VA, Moxson VS, et al. Low cost blended elemental titanium powder metallurgy. TITANIUM 2007, 2007, Orlando (Florida).
- [9] William HP, Blue CA, Kiggans JO, et al. Powder metallurgy and solid state processing of armstrong titanium and titanium alloy powders, 2007.
- [10] Levano O, Weston N, Pope J, et al. FAST- forge of novel Ti-6Al-4V/Ti-6Al-2Sn-4Zr-2Mo bonded, near net shape forgings from surplus AM powder. MATEC Web Conf. 2020;321:03010. doi:10.1051/mateconf/202032103010
- [11] Weston NS. A novel solid-state processing route to generate cost-effective titanium alloy components, 2017, 195.
- [12] Weston N, Derguti F, Jackson M. Exploitation of spark plasma sintering and one-step forging for cost-effective processing of titanium alloy powders. Proceedings of the 13th World Conference on Titanium. 2016:123–128. doi:10.1002/9781119296126.ch18
- [13] Weston NS, Thomas B, Jackson M. Exploitation of field assisted sintering technology (FAST) for titanium alloys. MATEC Web Conf. 2020;321:02006. doi:10.1051/mateconf/202032102006
- [14] Yolton CE, Froes FH. 2 - Conventional titanium powder production. Titanium Powder Metallurgy, Science, Technology and Applications; 2016:21–32.
- [15] Nesterenko VF, Goldsmith W, Indrakanti SS, et al. Response of hot isostatically pressed Ti-6Al-4V targets to normal impact by conical and blunt projectiles. Int J Impact Eng. 2003;28:137–160. doi:10.1016/S0734-743X(02)00052-0
- [16] Nesterenko VF, Indrakanti SS, Brar SN, et al. Ballistic performance of hot isostatically pressed (Hlped) Ti-based targets. Key Eng Mater. 2000;177-180:243–248. doi:10.4028/www.scientific.net/KEM.177-180.243
- [17] Weston NS, Thomas B, Jackson M. Processing metal powders via field assisted sintering technology (FAST): a critical review. Mater Sci Technol. 2019;35:1306–1328. doi:10.1080/02670836.2019.1620538
- [18] Lütjering G. Influence of processing on microstructure and mechanical properties of ($\alpha+\beta$) titanium alloys. Mater Sci Eng, A. 1998;243:32–45. doi:10.1016/S0921-5093(97)00778-8
- [19] Semiatin SL, Seetharaman V, Weiss I. The thermomechanical processing of alpha/beta titanium alloys. JOM. 1997;49:33–39. doi:10.1007/BF02914711
- [20] Weiss I, Semiatin SL. Thermomechanical processing of alpha titanium alloys – an overview. Mater Sci Eng, A. 1999;263:243–256. doi:10.1016/S0921-5093(98)01155-1
- [21] Gooch WA, Jr. Potential applications of titanium alloys in armor systems. Titanium. 2011;2011:1–22.
- [22] Schoenfeld SE, Kad B. Texture effects on shear response in Ti-6Al-4V plates. Int J Plast. 2002;18:461–486. doi:10.1016/S0749-6419(01)00005-5
- [23] Malik A, Nazeer F, Wang Y. A prospective way to achieve ballistic impact resistance of lightweight magnesium alloys. Metals. 2022;12:125. doi:10.3390/met12010125
- [24] Zheng C, Wang F, Cheng X, et al. Failure mechanisms in ballistic performance of Ti-6Al-4V targets having equiaxed and lamellar microstructures. Int J Impact Eng. 2015;85:161–169. doi:10.1016/j.ijimpeng.2015.06.017
- [25] Zheng C, Wang F, Cheng X, et al. Effect of microstructures on ballistic impact property of Ti-6Al-4V targets. Mater Sci Eng, A. 2014;608:53–62. doi:10.1016/j.msea.2014.04.032
- [26] Liu X, Tan C, Zhang J, et al. Correlation of adiabatic shearing behavior with fracture in Ti-6Al-4V alloys with different microstructures. Int J Impact Eng. 2009; 36:1143–1149. doi:10.1016/j.ijimpeng.2008.12.007
- [27] Gu Y. Ballistic testing and high-strain-rate properties of hot isostatically pressed Ti-6Al-4V, 1294, 2003, 1294–1297. <https://doi.org/10.1063/1.1483776>.
- [28] Kad BK, Schoenfeld SE, Burkins MS. Through thickness dynamic impact response in textured Ti-6Al-4V plates. Mater Sci Eng, A. 2002;322:241–251. doi:10.1016/S0921-5093(01)01135-2
- [29] Weston NS, Jackson M. FAST- forge – A new cost-effective hybrid processing route for consolidating titanium powder into near net shape forged components. J Mater Process Technol. 2017;243:335–346. doi:10.1016/j.jmatprotec.2016.12.013
- [30] Weston NS, Derguti F, Tudball A, et al. Spark plasma sintering of commercial and development titanium alloy powders. J Mater Sci. 2015;50:4860–4878. doi:10.1007/s10853-015-9029-6
- [31] MIL-DTL-46077G, Armor plate, Titanium alloy, Weldable, 2006.
- [32] Bachmann F, Hielscher R, Schaeben H. Texture analysis with MTEX – free and open source software toolbox. Solid State Phenom. 2010;160:63–68. doi:10.4028/www.scientific.net/SSP.160.63
- [33] Jackson M, Boyer RR. Titanium and its alloys: processing, fabrication and mechanical performance. Encycl Aersp Eng. 2010: 1–16. doi:10.1002/9780470686652.eae199
- [34] Wang YN, Huang JC. Texture analysis in hexagonal materials. Mater Chem Phys. 2003;81:11–26. doi:10.1016/S0254-0584(03)00168-8
- [35] Fisher ES, Renken CJ. Single-crystal elastic moduli and the hcp \rightarrow bcc transformation in Ti, Zr, and Hf. Phys Rev. 1964;135:A482–A494. doi:10.1103/PhysRev.135.A482
- [36] Titanium Metals Corporation, TIMETAL 6-4, 6-4 ELI, 6-4-.1Ru, Alloy Digest. 56, 2007, 5–6. doi:10.31399/asm.ad.ti0143